International Journal of Geo-Information

MDPI

Article

Dynamic Supply–Demand Matching and Spatial Mismatch Diagnosis of Emergency Beds in Designated Hospitals During Public Health Emergencies: A SEIQRDP-SG and 3SFCA-SMI Framework

Ying Zhong [1], Sheng Jiao [1,2,*], Qingqing Zhang [1] and Yizhe Ying [1]

[1] School of Architecture and Planning, Hunan University, Changsha 410082, China; zhongy0527@hnu.edu.cn (Y.Z.); zhangqingqing2023@hnu.edu.cn (Q.Z.)
[2] Hunan Engineering Technology Research Center for Smart Disaster Prevention and Resilient City Construction, Hunan University, Changsha 410082, China
* Correspondence: jiaosheng2008@163.com

Abstract

In the context of public health emergencies (PHEs), conventional static indicators are insufficient for capturing the dynamic supply–demand relationship of emergency medical care. Grounded in adaptive cycle theory, this study proposes a integrated analytical framework that sequentially integrates supply baseline identification, disturbance impact simulation, mismatch diagnosis, and zoning-based response optimization. Taking 475 communities and 18 major designated hospitals in the Changsha metropolitan area as the empirical case, we integrate AHP-CRITIC evaluation, the SEIQRDP-SG model, and the 3SFCA-SMI method to identify the spatial mismatch of emergency-bed supply and demand and to delineate planning response zones. The results show that: (1) emergency-bed supply exhibits marked agglomeration and quasi-Pareto polarization, with the top three districts accounting for 75.83% of effective emergency beds; (2) under the core scenario of $R_0 = 5$ with moderate intervention, peak bed demand in the metropolitan area reaches approximately 7835 beds around day 21, with high-demand communities emerging in high-density and high-mobility areas; and (3) although the overall supply–demand ratio is 1.34, 78% of communities cannot reach any designated hospital within 15 min, and the supply–demand pattern forms a compound spatial structure characterized by "central carrying, transitional mismatch, and peripheral weakness". These findings indicate that the primary constraint on emergency medical resilience lies not in aggregate bed shortages alone, but in structural spatial mismatch jointly shaped by effective supply, dynamic demand, and transfer-time constraints. This study extends emergency medical facility evaluation from static assessment to dynamic matching and provides evidence for the layout of resilient "dual-use" medical facilities for routine and emergency conditions.

Keywords: adaptive cycle; emergency medical care; designated hospital; SEIQRDP-SG; supply–demand matching; spatial accessibility; Changsha

Check for updates

Academic Editors: Wolfgang Kainz, Lan Mu and Jue Yang

Received: 23 June 2026
Revised: 27 July 2026
Accepted: 30 July 2026
Published: 1 August 2026

Copyright: © 2026 by the authors. Published by MDPI on behalf of the International Society for Photogrammetry and Remote Sensing. Licensee MDPI, Basel, Switzerland. This article is an open access article distributed under the terms and conditions of the Creative Commons Attribution (CC BY) license.

1. Introduction

Public health emergencies (PHEs) impose pressures on urban healthcare systems that exceed routine service capacity and operational logic [1]. Such events have demonstrated that an adequate static aggregate supply of urban medical resources does not necessarily

translate into effective accessibility or equitable allocation under sudden disturbances [2–4]. Rapid short-term increases in infected individuals, quarantined populations, and hospitalization demand may transform an originally stable healthcare service network into a highly dynamic supply–demand coupling system. In some areas, risks of healthcare system overload may emerge due to the combined effects of concentrated bed resources, constraints on patient transfer, heterogeneous population exposure, and overlapping demand peaks [5,6]. To address challenges to urban resilience, the Chinese government introduced the strategy of "dual-use for routine and emergency conditions" infrastructure in 2023 [7], explicitly requiring medical facilities to reserve emergency response capacity while fulfilling routine service functions. Within China's hierarchical and classified emergency medical treatment system [8,9], primary healthcare institutions (PHCIs) are responsible for monitoring, early warning, and referral coordination; Fangcang shelter hospitals or temporary treatment facilities are used to admit mild cases; and designated hospitals are assigned the central role of treating critically ill patients [10]. Among these facilities, designated hospitals serve as core nodes for critical-care resources. Their ability to match available capacity with surge demand directly determines the surge-capacity ceiling of the urban emergency healthcare system [11–13]. However, existing planning frameworks still tend to evaluate such facilities mainly through static aggregate resource coordination, while paying insufficient attention to the dynamic response capacity and spatial mechanisms through which facility quantity is transformed into emergency timeliness under sudden disturbances [14,15].

Supply–demand matching (SDM) of medical facilities has long been an important topic in health geography, urban planning, and public health research [16]. Traditional assessments often relied on provider-to-population ratios and aggregate indicators, such as the numbers of hospital beds, physicians, and medical resources per capita. However, these measures cannot adequately capture spatial impedance or competition for limited healthcare services [17]. With advances in geographic information system (GIS)-based spatial analysis, the two-step floating catchment area (2SFCA) method has become a fundamental approach because it jointly considers healthcare supply, population demand, and travel-time catchments [18]. Nevertheless, conventional 2SFCA assumes uniform accessibility within a catchment and fixed catchment boundaries and may overestimate demand when the service areas of multiple facilities overlap [19]. To address these issues, subsequent studies introduced distance-decay weighting [20] and variable catchment sizes [21,22], while others incorporated dynamic travel times [23,24] or facility configuration effects (M2SFCA) [25]. To explicitly tackle the overlap-induced overestimation, Wan et al. proposed the 3SFCA method with a competition-adjustment step [26]. Later Huff-based extensions added travel impedance and facility attractiveness to represent probabilistic choice [27]. Building on these, the MH3SFCA method integrates Huff interaction probabilities with continuous distance decay to better capture patient choice behavior [28].

Unlike routine healthcare settings, acute infectious-disease outbreaks such as COVID-19 can rapidly reshape the spatial relationship between healthcare supply and demand. Accordingly, research has gradually expanded from routine accessibility assessment to emergency healthcare accessibility and equity during PHEs, including dynamic accessibility to intensive care unit (ICU) beds, temporary healthcare facility location, and resource allocation during epidemic peaks [14,29,30]. Existing studies have demonstrated that healthcare accessibility under PHEs is inherently dynamic rather than static. In such contexts, patients are typically transferred under designated treatment arrangements and substantial time constraints rather than freely selecting facilities based on facility attractiveness [31]. Therefore, the present study adopts the conventional 3SFCA method to retain the representation of facility competition and reduce potential supply–demand overestimation, while avoiding strong assumptions regarding subjective facility-choice behavior under crisis

conditions. Meanwhile, infectious-disease models have been widely applied to simulate epidemic transmission and have increasingly incorporated spatial heterogeneity associated with population mobility, the built environment, and intervention policies [32,33]. Overall, the literature reflects a transition from static resource allocation toward dynamic network analysis and from individual facility sitting toward system-level resilience. Nevertheless, three major limitations remain. First, supply measurement still relies heavily on static indicators, such as facility hierarchy and bed capacity, making it difficult to accurately characterize effective supply capacity under emergency conditions. Second, existing models do not sufficiently integrate complex mechanisms such as the spatially heterogeneous evolution of emergency demand and competition for healthcare resources. Third, analytical applications often remain limited to describing spatial patterns or estimating aggregate deficits, with insufficient translation of diagnostic results into a closed-loop framework for zoning-based intervention.

To address these gaps, this study takes the Changsha metropolitan area, China, as the study area and, drawing on adaptive cycle theory, develops an analytical framework for the dynamic SDM of urban emergency medical facilities. The framework comprises four sequential components: identifying the supply base, simulating disturbance shocks, diagnosing supply–demand mismatches, and optimizing zoning-based responses. By integrating effective emergency supply assessment, SEIQRDP-SG-based demand simulation, and accessibility-based spatial mismatch diagnosis, the study aims to reveal why the aggregate availability of hospital beds does not necessarily translate into timely and spatially accessible emergency treatment capacity during PHEs, and to identify priority areas for differentiated planning interventions.

2. Materials and Methods

2.1. Conceptual Framework

The adaptive cycle is an important framework in resilience theory for explaining the evolutionary dynamics of complex systems. It emphasizes that systems evolve cyclically through resource accumulation, structural consolidation, disturbance-induced release, and adaptive reorganization. The adaptive cycle consists of four interconnected phases: exploitation (r), conservation (K), release (Ω), and reorganization (α) [34]. Unlike the perspective of static equilibrium, the adaptive cycle focuses more on how system vulnerabilities are exposed under external shocks and how new adaptive states are achieved through structural adjustment [34,35]. Urban emergency medical facility systems exhibit typical characteristics of complex adaptive systems [36,37]. Under routine conditions, the spatial configuration of facilities and the built environment (BE) constitute the system's underlying base. Once a public health emergency disrupts the original equilibrium, the scale of demand, healthcare-seeking flows, and modes of resource allocation may change rapidly within a short period. This shock forces the relatively stable supply–demand relationship under routine conditions to transform quickly into a dynamic matching problem under emergency conditions [38,39], thereby compelling the system to undergo reorganization and functional adaptation. Therefore, the adaptive cycle provides an appropriate theoretical lens for characterizing the evolutionary process of emergency medical supply–demand relations, namely "accumulation–consolidation–imbalance–reorganization" [40,41].

Based on this logic, this study translates the analytical pathway of emergency medical SDM into four sequential components: supply measurement, demand simulation, matching diagnosis, and zoning-based response (Figure 1). Each component is explicitly linked to the corresponding phase of the adaptive cycle. In the exploitation phase, potential capacity is quantified by constructing a comprehensive evaluation system to accurately measure the effective emergency supply capacity of designated hospitals. For the conservation and re-

lease phases, the BE is incorporated to characterize the spatiotemporal changes in demand scale and the SDM relationship under disturbance. The BE under routine conditions may be transformed into spatial conditions that amplify demand during disturbances. Within a specific travel-time threshold and under road-network constraints, this study quantifies the spatial coupling between community-level "demand flows" and the "supply fields" of designated hospitals, thereby accurately identifying key nodes of systemic healthcare overload and supply–demand mismatch. In the reorganization phase, the results of mismatch identification are transformed into targets for spatial planning response. Differentiated response zones are classified according to supply–demand combinations and the degree of mismatch, and planning intervention directions are specified for each zone.

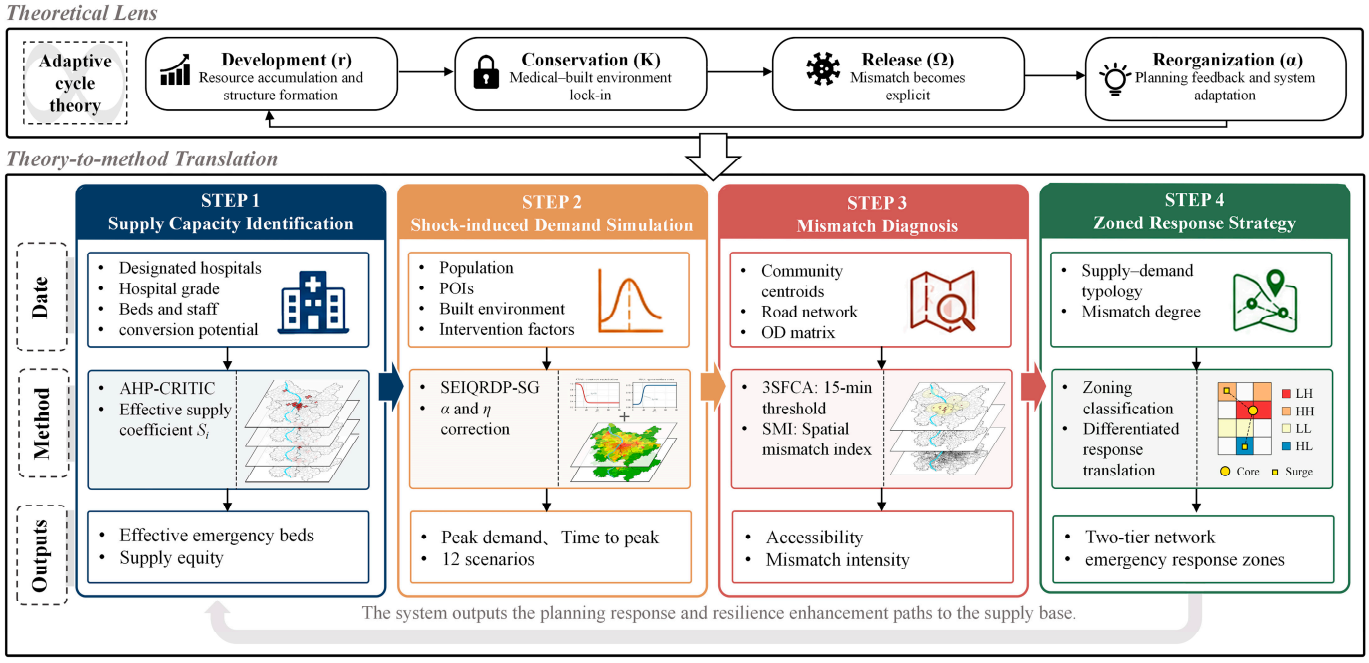


Figure 1. Conceptual and methodological framework.

2.2. Study Area and Data

2.2.1. Study Area

This study takes the Changsha metropolitan area as the study area (Figure 2). Changsha, the capital city of Hunan Province and a megacity in central China, is characterized by a high concentration of medical resources, pronounced spatial differentiation of population distribution, and frequent cross-district healthcare-seeking interactions, making it highly representative of megacities in central China. The study area covers the entire administrative areas of Furong, Tianxin, Kaifu, and Yuhua districts, as well as parts of Wangcheng District, Yuelu District, and Changsha County, with a total area of approximately 2100 km^2. Communities are used as the basic analytical units in this study, comprising 475 units in total, and their weighted centroids are adopted as spatial anchors of demand.

2.2.2. Data Sources and Preprocessing

The datasets used in this study were grouped into four categories: geospatial data, medical and healthcare data, population data, and built-environment (BE) and points-of-interest (POIs) data.

Geospatial data. These data include the metropolitan area boundary, district and county boundaries, community boundaries, and the road network. Administrative and community boundaries at different levels were obtained from the Resource and Environment Science and Data Center of the Chinese Academy of Sciences (https://www.resdc.cn/,

accessed on 10 January 2026). Road-network data were obtained from OpenStreetMap (https://www.openstreetmap.org/, accessed on 10 January 2026). After acquisition, the spatial datasets were transformed to a common coordinate system, clipped to the study area, and checked for topological consistency. A total of 475 communities were retained as the basic spatial analytical units.

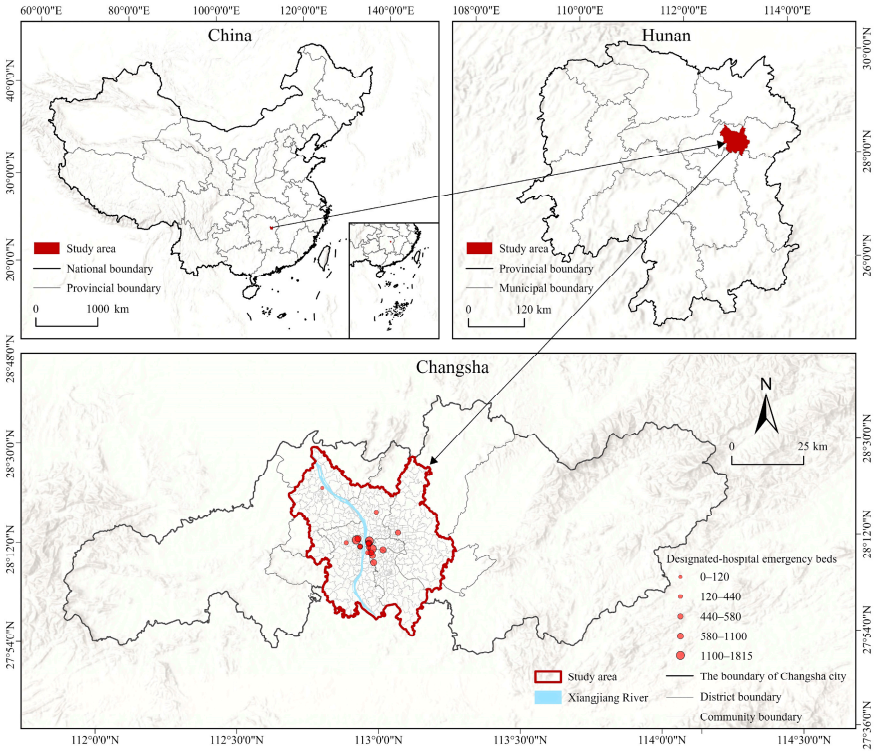


Figure 2. Location of the study area.

Medical and healthcare data. These data include the list of designated hospitals, hospital tiers, approved bed capacity, and numbers of medical staff. Hospital attribute data were compiled from publicly available information released by the Changsha Municipal Health Commission and from the annual reports of individual hospitals, while hospital locations were obtained from the Gaode Maps API (https://ditu.amap.com/, accessed on 10 January 2026). Hospital records were matched and cross-validated based on hospital names, addresses, and geographic locations. A total of 18 designated hospitals were included in the study area, comprising 16 Grade III Class A hospitals and 2 Grade III Class B hospitals. By hospital type, these included 12 general hospitals, 4 traditional Chinese medicine hospitals, and 2 specialized hospitals. Collectively, the 18 hospitals provided 13,895 beds and employed 28,597 medical staff. These data were subsequently used to evaluate hospital emergency supply capacity and estimate the effective supply of emergency beds.

Population data. Population data include both permanent resident population and older adult population. The permanent resident population data were obtained from the 100 m gridded population dataset of China's Seventh National Population Census [42]. After clipping to the study area and aggregation to the community scale, the total permanent resident population across the 475 communities was 6,766,397. Data on the population aged 65 years and older were obtained from WorldPop (https://www.worldpop.org/, accessed on 10 January 2026), calibrated according to the age structure reported in the Seventh National Population Census, and aggregated to the community scale. The study area contained approximately 706,700 residents aged 65 years and older.

BE and POIs data. Relevant data were primarily obtained from the Gaode Maps API (https://ditu.amap.com/, accessed on 10 January 2026). A total of 5920 residential communities, comprising 3,959,273 households, were identified. Among them, 1064 were classified as old residential communities, urban villages, or shantytowns, comprising 419,970 households. After removing duplicate and invalid records and completing functional classification and spatial matching, the final dataset included 883 grassroots governance facilities, comprising neighborhood committee offices and community service centers, 7217 public transport stops, 7782 commercial facilities, 1274 high-risk venues, and 2268 activity spaces for susceptible groups.

2.3. Methods

Based on adaptive cycle theory, this study systematically evaluates the dynamic matching relationship of emergency beds in designated hospitals in the Changsha metropolitan area during PHEs along the pathway of "supply measurement–demand simulation–matching diagnosis–zoning response".

2.3.1. Supply Side Measurement

In the context of PHEs, the actual treatment capacity of designated hospitals is jointly constrained by their comprehensive treatment capacity and their routine-to-emergency conversion potential [43,44]. In this study, the number of effective emergency beds was used to represent the actual supply capacity. First, the upper limit of convertible beds was determined based on the existing bed capacity of each hospital [45]. Then, a comprehensive evaluation system was constructed from two dimensions, namely "treatment capacity" and "emergency capacity" (Table 1). All selected indicators represent medical-resource endowment or routine-to-emergency conversion potential, with higher values indicating stronger emergency supply capacity; therefore, they were treated as benefit-type indicators. The AHP–CRITIC combined weighting method was adopted to avoid the subjectivity associated with a single weighting approach. The effective supply capacity coefficient C_i of each hospital was calculated using Equation (1):

$$C_i = \sum_{j=1}^{m} w_j x'_{ij} \quad (1)$$

where w_j denotes the combined weight of the j-th indicator, and x'_{ij} denotes the standardized value of the indicator. Based on this coefficient, the number of effective emergency beds in each designated hospital was estimated.

Table 1. Indicator system for the treatment–emergency capacity evaluation.

Criterion Layer	Indicator Layer	Data Source	AHP Weight	CRITIC Weight	Combined Weight
Treatment capacity	Hospital tier	Changsha Municipal Health Commission	0.088	0.232	0.160
	Total number of medical staff	Annual hospital reports	0.158	0.264	0.211
Emergency capacity	effective emergency beds	Xiang Medical Insurance WeChat-program, and annual hospital reports	0.482	0.234	0.358
	Potential for "three zones and two passages" renovation	Hospital architectural plans and relevant expansion plans	0.272	0.269	0.271

2.3.2. Demand-Side Simulation

(1) Model Specification and Equations

Emergency medical demand during PHEs is not a static mapping of the routine population. Instead, it emerges dynamically with epidemic transmission and exhibits substantial spatial heterogeneity [46–48]. To capture this process, this study extends the classical SEIR model in two ways and develops a spatially corrected and government-intervened SEIQRDP-SG model, namely Susceptible–Exposed–Infectious–Quarantined–Recovered–Deceased–Protected [49]. First, three additional compartments are introduced: quarantined/admitted individuals (Q), deceased individuals (D), and protected individuals (P). For designated-hospital bed-demand estimation, Q is operationally defined as admitted in-treatment cases occupying emergency beds rather than all quarantined or detected cases; mild or asymptomatic cases managed through temporary or non-designated facilities are not included in the modeled bed demand. Second, a BE spatial correction coefficient α and a heterogeneous governance intervention coefficient η are introduced to characterize the spatial differentiation of transmission rates and the community-level variation in intervention intensity, respectively.

For community i, the total population is represented by its permanent resident population N_i. The evolution of population states is described by the system of ordinary differential equations in Equation (2):

$$\begin{cases} \frac{dS_i}{dt} = -\beta_i(t)\frac{S_i I_i}{N_i} - \xi_i(t)(1 - G(t))S_i \\ \frac{dE_i}{dt} = \beta_i(t)\frac{S_i I_i}{N_i} - \sigma E_i \\ \frac{dI_i}{dt} = \sigma E_i - \delta_i(t) I_i - \gamma I_i \\ \frac{dQ_i}{dt} = \delta_i(t) I_i - \lambda Q_i - \kappa Q_i \\ \frac{dR_i}{dt} = \lambda Q_i + \gamma I_i \\ \frac{dD_i}{dt} = \kappa Q_i \\ \frac{dP_i}{dt} = \xi_i(t)(1 - G(t))S_i \end{cases} \quad (2)$$

where σ is the transition rate from exposed to infectious; γ is the self-recovery rate of infectious individuals; λ is the recovery rate of quarantined/admitted individuals; κ is the disease fatality rate; and $\beta_i(t)$, $\delta_i(t)$, and $\xi_i(t)$ denote the time-varying transmission rate, admission/isolation rate, and self-protection transition rate of community i, respectively. Key parameters were specified based on previous epidemiological studies (Table 2).

Table 2. Basic parameter settings of the SEIQRDP-SG model.

Parameter Symbol	Parameter Name	Value
R_0	Basic reproduction number	1.5, 3.0, 5.0 [50,51]
σ	Transition rate from exposed to infectious	1/5.2 [52]
γ	Self-recovery rate of infectious individuals	1/14 [53,54]
λ	Recovery rate of quarantined/admitted individuals	1/10 [55,56]
κ	Disease fatality rate	0.005 [57]
T	Simulation period	150 days

(2) Spatiotemporal Heterogeneity Correction and Government Intervention

Micro-scale spatial resistance and policy effects were captured by introducing a spatial correction coefficient and a government intervention function into the model (Figure 3). The spatial differentiation of the transmission rate was represented by the built-environment correction coefficient α, which consists of two dimensions: contact frequency $\alpha_{\text{freq},i}$ and infection probability $\alpha_{\text{prob},i}$ [58–60]. The frequency dimension includes factors that reflect

contact opportunities and mobility intensity, such as population density, public transport density, commercial vitality, high-risk facility density, and the density of activity spaces for susceptible groups. The probability dimension includes factors that reflect infection amplification risks, such as the proportion of older adults, the proportion of old residential areas, urban villages, shantytowns, and road network density (Table 3). Objective weights were determined using the entropy weight method and then integrated. After normalization, the time-varying transmission rate of community i is specified as in Equation (3):

$$\beta_i(t) = \beta_0 \cdot \alpha_{\text{freq},i} \cdot \alpha_{\text{prob},i} \cdot G_i(t) \tag{3}$$

where β_0 denotes the baseline transmission rate, calibrated according to the target R_0 in each scenario; and $G_i(t)$ denotes the contact-suppression function under government intervention. Under the baseline condition without intervention, and with the mean value of the spatial correction coefficient normalized to 1, β_0 was calibrated according to the target R_0, so that the effective reproduction number in the initial stage of the model was consistent with the specified scenario.

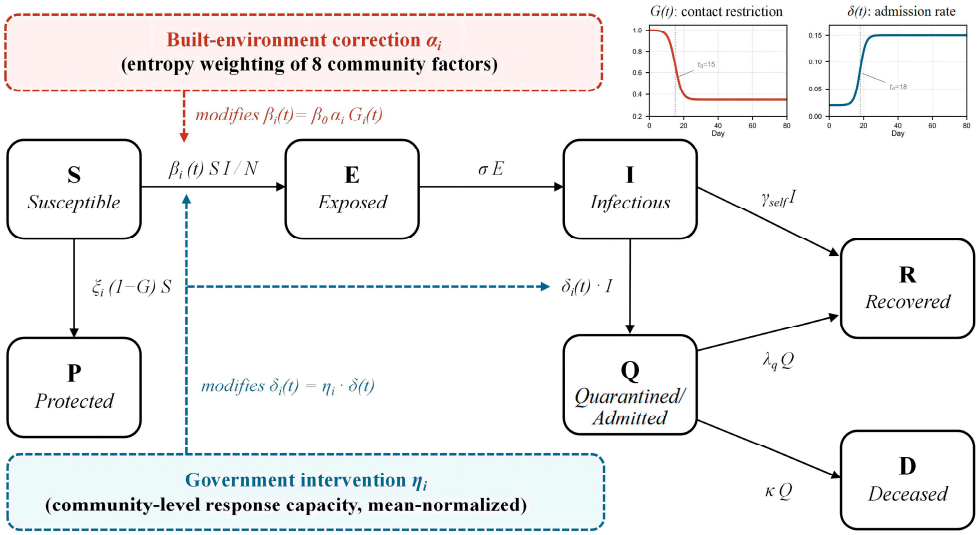


Figure 3. Structure of the SEIQRDP-SG model.

Table 3. Indicators of spatial correction factors.

Criterion Layer	Meaning	Indicator Layer	Meaning
Transmission frequency	Represents contact opportunities and mobility intensity within communities, affecting the potential transmission range	Population density	Ratio of permanent resident population to community area
		Public transport stop density	Kernel density of bus stops and metro stations
		Commercial facility density	Kernel density of shopping malls, supermarkets, markets, and other commercial facilities
		High-risk venue density	Kernel density of infectious disease hospitals, wholesale markets, fresh food markets, and other high-risk venues
		Density of activity spaces for susceptible groups	Kernel density of nursing homes, kindergartens, primary schools, and other facilities frequently used by susceptible groups
Transmission probability	Represents the amplification effect of population structure and spatial environment on infection diffusion risk	Proportion of older adults	Share of residents aged 65 and above in the permanent resident population
		Proportion of old residential areas, urban villages, and shantytowns	Ratio of relevant residential land area to total community area
		Road density	Ratio of total road length to community area

Government intervention was jointly characterized by the contact-suppression function $G(t)$ and the admission rate $\delta(t)$ [61,62]. Specifically, $G(t)$ decreases over time from 1 to the lower bound $G_{\min}$, representing the suppression of contact frequency caused by strengthened control measures. The admission/isolation rate $\delta(t)$ increases over time from the baseline level to the upper bound δ_{cap}, representing the gradual improvement of testing and isolation capacity. To further characterize differences in the implementation of unified policies at the community scale, the spatial supply level of neighborhood committees and community centers was used as a proxy for grassroots governance response capacity. After density transformation and mean normalization, the heterogeneous intervention coefficient η_i was constructed. The actual intervention effects for community i are given by Equations (4) and (5):

$$G_i(t) = G(t)^{\eta_i} \tag{4}$$

$$\delta_i(t) = \min\left[\eta_i \cdot \delta(t), \delta_{cap}\right] \tag{5}$$

where $\eta_i > 1$ indicates that the community governance response capacity is higher than the citywide average, resulting in stronger contact suppression and higher isolation-transfer efficiency. Conversely, $\eta_i < 1$ indicates relatively weaker response capacity.

(3) Definition of Bed Demand and Scenario Settings

Medical bed demand was no longer estimated through a static conversion using a fixed rate. Instead, it was endogenously derived from the Q compartment of the model [63,64]. In this study, $Q_i^s(t)$ is defined as the number of admitted in-treatment individuals occupying emergency beds in community i under scenario s. Therefore, its peak value can be directly used as the theoretical peak of bed demand B_i^s, as shown in Equation (6):

$$B_i^s = \max_{t\in[0,T]} Q_i^s(t) \tag{6}$$

To systematically examine the effects of transmission intensity and intervention strength on demand, twelve orthogonal scenarios were established by combining three levels of the basic reproduction number ($R_0 = 1.5, 3.0, 5.0$) with four levels of intervention intensity: S1, no intervention; S2, weak intervention; S3, moderate intervention; and S4, strong intervention. These intervention levels were jointly regulated by $G_{\min}$, δ_{lift}, and η. The simulation period was set to 150 days (Table 4). Among these scenarios, $R_0 = 5.0$ was used to represent a high-transmission epidemic scenario [65,66]. This value was adopted as a stress-test parameter rather than an exact estimate for a specific outbreak in Changsha. Accordingly, $R_0 = 5.0$ combined with moderate intervention (S3) was selected as the core scenario for subsequent SDM diagnosis under substantial epidemic pressure.

2.3.3. Supply–Demand Matching

(1) Measurement of Emergency Bed Accessibility Based on the 3SFCA

The methodological rationale for adopting 3SFCA was established through a comparison with the Modified Huff Three-Step Floating Catchment Area (MH3SFCA) method in terms of model structure, facility-choice assumptions, computational complexity, and applicability (Table 5). Given the designated transfer arrangements and constrained patient choice during PHEs, the more parsimonious 3SFCA method was adopted. Community weighted centroids and designated hospitals were used as demand and supply points, respectively.

Table 4. Scenario settings of transmission intensity and intervention strength.

Dimension	Scenario Type	Parameter Value	Meaning
R_0 level	Low	1.5	Low transmission pressure
	Medium	3.0	Medium transmission pressure
	High	5.0	High transmission pressure
Intervention level	S1, no intervention	$G_{min} = 1.00, \delta_{\text{lift}} = 0.00, t_0 = -, t_{\text{end}} = -$	Baseline without control measures
	S2, weak	$G_{min} = 0.60, \delta_{\text{lift}} = 0.08, t_0 = 20, t_{\text{end}} = 25$	Limited contact reduction with relatively delayed strengthening of testing, case identification, isolation, and admission/transfer capacity.
	S3, moderate	$G_{min} = 0.35, \delta_{\text{lift}} = 0.13, t_0 = 15, t_{\text{end}} = 18$	Moderate contact reduction combined with enhanced testing and earlier case identification, isolation, and admission/transfer response.
	S4, strong	$G_{min} = 0.15, \delta_{\text{lift}} = 0.18, t_0 = 10, t_{\text{end}} = 12$	Intensive and early contact reduction combined with rapid testing, isolation, and coordinated admission/transfer response.

Table 5. Comparison of 3SFCA and MH3SFCA for emergency medical accessibility assessment.

Dimension	3SFCA	MH3SFCA
Model structure	Allocates demand using normalized travel-time decay and accounts for competition among reachable facilities.	Uses capacity-weighted Huff interaction probabilities together with continuous distance-decay weights.
Underlying assumption	Demand allocation is governed primarily by relative travel impedance.	Patient–facility interaction is jointly influenced by facility capacity and travel impedance.
Computational complexity	Relatively parsimonious, with one normalized impedance weight for each reachable OD pair.	More complex, requiring both Huff interaction probabilities and separate distance weights for each OD pair.
Applicability	More suitable for designated, time-constrained emergency transfer with limited patient choice.	More suitable when capacity-sensitive and discretionary facility choice needs to be represented.

Under road-network constraints, a 15 min catchment was used to represent emergency transfer efficiency and the cross-district service characteristics of high-tier hospitals. This threshold measures potential road-network accessibility rather than total prehospital or door-to-treatment time, because emergency-call processing, ambulance dispatch, on-scene triage and stabilization, real-time traffic, and hospital handover were not explicitly modeled owing to the lack of consistent community-level data [67,68]. Robustness was further assessed using 20 and 30 min thresholds. A Gaussian time-decay function was used to calculate the probability that community i selects hospital j:

$$f(t_{ij}) = \exp\left[-\frac{1}{2} \cdot \left(\frac{t_{ij}}{t_0}\right)^2\right] \tag{7}$$

The choice probability P_{ij}, the supply–demand ratio R_j^s of hospital j under scenario s, and the comprehensive accessibility A_i^s of community i were then calculated using Equations (8)–(10):

$$P_{ij} = \frac{f(t_{ij})}{\sum_k f(t_{ik})}, \ (t_{ik} \le t_0) \tag{8}$$

$$R_{js} = \frac{S_j}{\sum_i P_{ij} \cdot D_{is}}, \ (t_{ij} \le t_0) \tag{9}$$

$$A_i^s = \sum_j P_{ij} \cdot R_j^s \tag{10}$$

where t_{ij} denotes the travel time from community i to hospital j, and t_0 denotes the search threshold. P_{ij} denotes the probability that community i selects hospital j. R_j^s denotes the supply–demand ratio of hospital j under scenario s. A_i^s denotes the comprehensive accessibility obtained by community i under scenario s. A higher value of A_i^s indicates that more abundant emergency bed resources are available to the community within the given travel-time constraint.

(2) Quantification of Spatial Mismatch and Zoning Classification Based on SMI

To further quantify the direction and intensity of supply–demand deviation, accessibility and bed demand under each scenario s were standardized using Z-scores, and the spatial mismatch index (SMI) was constructed [69,70], as shown in Equation (11):

$$SMI_i^s = Z(A_i^s) - Z(B_i^s) \tag{11}$$

where $SMI_i^s > 0$ indicates relatively sufficient supply, whereas $SMI_i^s < 0$ indicates higher demand pressure. A larger absolute value indicates a stronger degree of deviation. Based on the combination of standardized accessibility and standardized demand, accessible communities were further classified into four types of matching areas: priority mismatch zones with high demand and low supply, high-load zones with high demand and high supply, supply-surplus zones with low demand and high supply, and low-pressure weak zones with low demand and low supply. Communities that could not reach any designated hospital within 15 min were separately classified as accessibility blind zones.

3. Results

3.1. Spatial Differentiation in the Effective Supply Capacity of Designated Hospitals

In the exploitation phase of the adaptive cycle, the supply-side measurement was used to characterize the potential medical resource accumulated under routine conditions and its spatial distribution characteristics. According to the official list of designated hospitals released by the Changsha Municipal Health Commission, 18 designated hospitals were identified within the study area, with a total of 10,525 effective emergency beds.

The emergency medical supply in the Changsha metropolitan area exhibited pronounced hierarchy-dependent and spatially clustered characteristics. At the hospital scale, the Gini coefficient of the spatial distribution of effective emergency bed capacity was 0.367 (Figure 4a), indicating a relatively high level of concentration. The four largest Grade-A tertiary hospitals accounted for 47.1% of the total effective beds, thereby constituting the core nodes of emergency medical treatment. At the administrative-district scale, Yuelu, Kaifu, and Furong districts together accounted for 75.83% of the effective beds, far exceeding the theoretical equal-share value of 42.86% across the seven administrative units. This pattern closely resembled Pareto-like polarization and formed the core carrying belt of emergency medical resources. In contrast, Tianxin District, Wangcheng District, and Changsha County together accounted for less than 7%, forming a pronounced long tail of weak peripheral supply (Figure 4b).

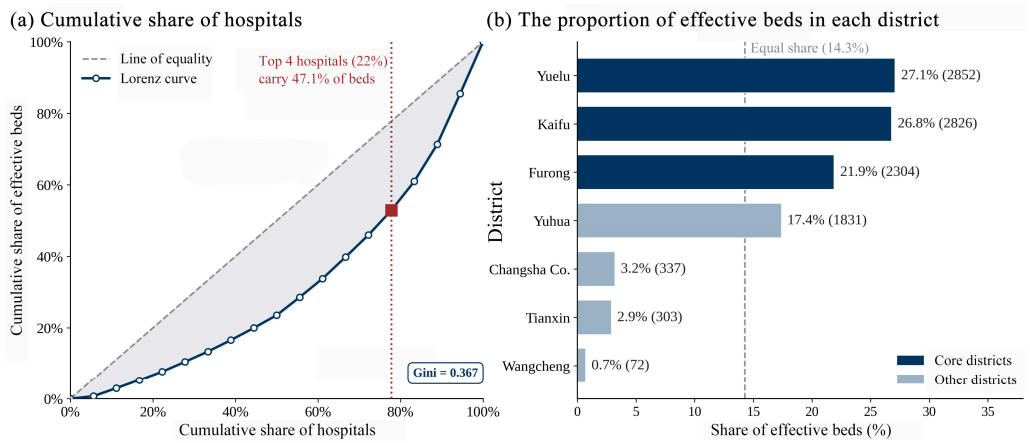


Figure 4. Spatial distribution and concentration of effective emergency bed capacity in designated hospitals; (**a**) cumulative share of hospitals; (**b**) the proportion of effective beds in each district.

This spatial pattern can be regarded as the cumulative outcome of the exploitation phase, during which medical resources have long been accumulated along administrative hierarchies and development intensity. Under routine conditions, economies of scale facilitate the intensive use of resources. However, they also create strong path dependence on a small number of core nodes. Once these core nodes become overloaded and cross-district coordination mechanisms are insufficient, vulnerabilities may rapidly spill over along the transport network and referral flows.

3.2. Spatiotemporal Evolution and Emergence of Emergency Bed Demand

3.2.1. Spatial Drivers of Demand Agglomeration

In the release phase of the adaptive cycle, once a public health emergency enters the system as a strong external disturbance, demand is not uniformly amplified according to population size. Instead, it is redistributed under the heterogeneous effects of the BE and government intervention intensity. A spatial correction coefficient, α, was constructed based on eight BE indicators and was used to spatially adjust the transmission rate. The multicollinearity test showed that the variance inflation factor (VIF) values of all indicators ranged from 1.003 to 4.242 (Table 6), indicating no significant multicollinearity.

Table 6. VIF test values of spatial correction factors.

Indicator	Population Density	Public Transport Stop Density	Commercial Facility Density	High-Risk Venue Density	Density of Activity Spaces for Susceptible Groups	Proportion of Older Adults	Proportion of Old Residential Areas, Urban Villages, and Shantytowns	Road Density
VIF value	1.003	4.030	4.242	1.320	3.213	1.034	1.198	1.998

In terms of spatial distribution (Figure 5a–h), high values of frequency-related indicators (Figure 5a–e) were highly concentrated in the core built-up area on the east bank of the Xiangjiang River, reflecting high-intensity population contact and mobility. High values of probability-related indicators (Figure 5f–h) were more frequently distributed in old urban areas and high-intensity development communities. The superposition of these two types of indicators resulted in an overall spatial pattern of α characterized by "central agglomeration and peripheral decline" (Figure 5i). The highest α values were observed in the core built-up area, indicating that its actual transmission potential was substantially amplified under the same baseline transmission rate.

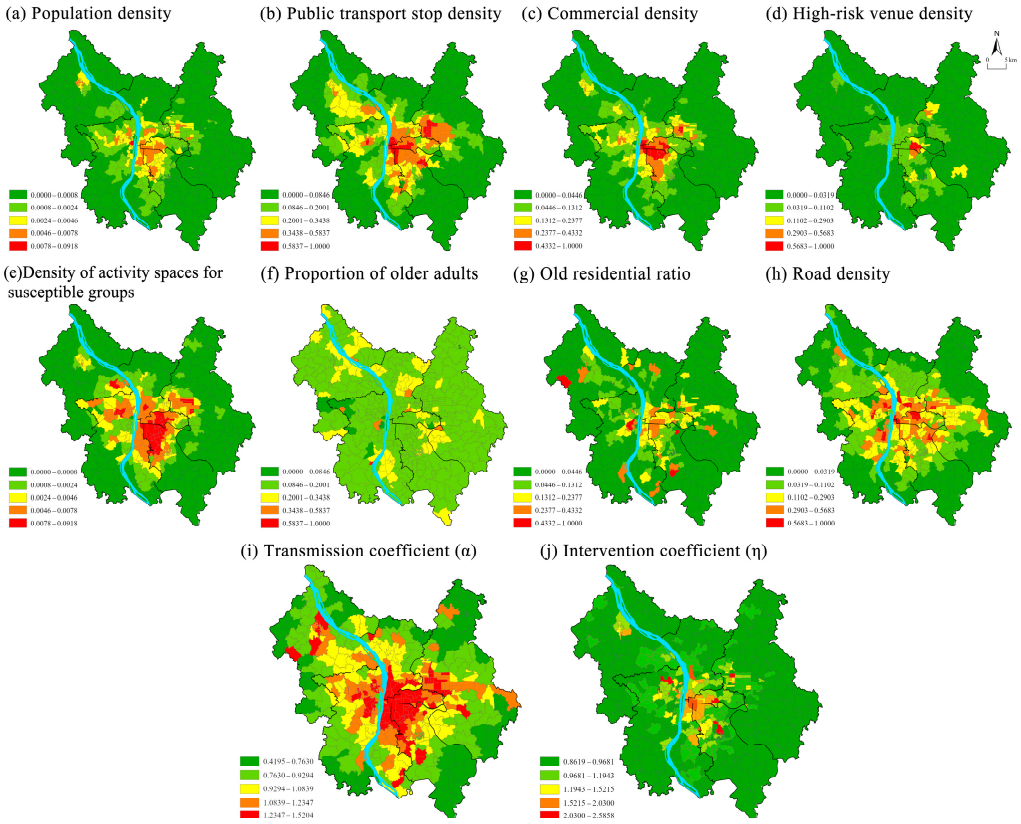


Figure 5. Spatial patterns of built-environment correction factors, the spatial correction coefficient α, and the governance intervention coefficient η: (**a**–**h**) built-environment correction factors; (**i**) spatial correction coefficient α; (**j**) governance intervention coefficient η.

The governance intervention coefficient η further captured spatial inequalities in community-level admission and control capacity (Figure 5j). The coefficient η not only affected the susceptible-to-exposed process (S→E) by regulating contact intensity but also acted on the infectious-to-quarantined/admitted process (I→Q) through the isolation and admission rate, thereby determining the capacity to effectively intercept demand and convert it into in-treatment bed demand. Together, α and η reshaped the relatively balanced demand expectation under routine conditions into a highly spatially differentiated pattern under emergency conditions. This constitutes the internal mechanism through which demand emerges from a homogeneous baseline into spatial agglomeration.

3.2.2. Scenario Responses of Demand Scale and Temporal Rhythm

The scale and temporal rhythm of demand were further jointly regulated by transmission intensity and intervention strength. Transmission intensity primarily determined peak magnitude, whereas intervention strength mainly controlled peak reduction and delay. Across the 12 scenario curves formed by three risk levels (R_0 = 1.5, 3, and 5) and four intervention intensities (S1: no intervention; S2: weak intervention; S3: moderate intervention; S4: strong intervention), the temporal curves of daily infections and in-treatment cases reflected the dynamic response process of the system under different disturbances (Figure 6).

In terms of curve morphology, both the infection curves and in-treatment curves under all scenarios display unimodal and right-skewed distributions, consistent with the outbreak pattern of PHEs under a finite population size. The peak of in-treatment cases lagged that of infections by approximately 3–5 days, reflecting the temporal delay from infection to symptom onset, testing, isolation, and admission. The stronger the intervention, the more

pronounced the lag became, as control measures slowed the transmission process and delayed the peak arrival time of both infections and in-treatment cases.

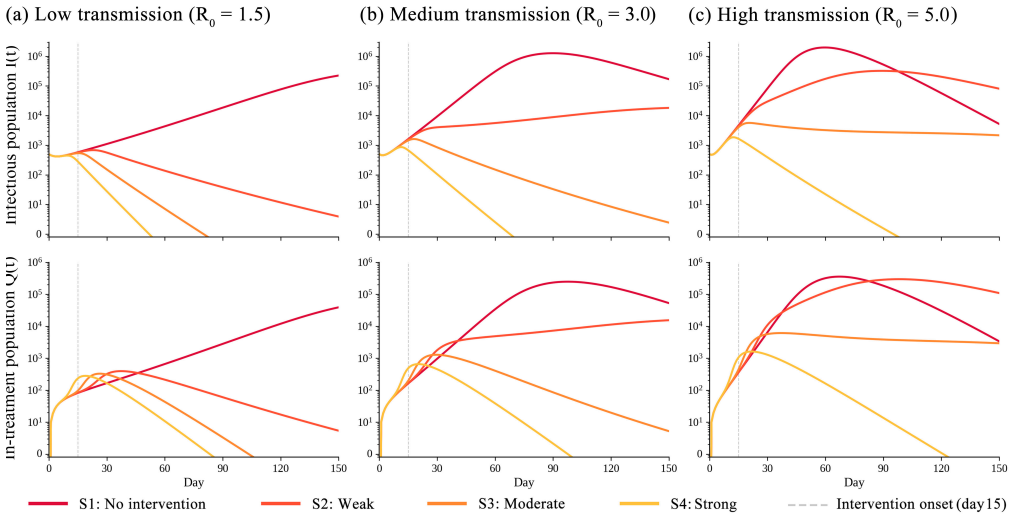


Figure 6. Temporal evolution of infectious and in-treatment populations under 12 scenarios: (**a**) low transmission (R_0 = 1.5); (**b**) medium transmission (R_0 = 3.0); (**c**) high transmission (R_0 = 5.0).

The concentration of emergency bed demand demonstrated strong structural robustness across scenarios. Regardless of changes in macro-level shock intensity and intervention strength, the top 10% of core high-pressure communities consistently accounted for 40–70% of citywide bed demand (Figure 7). This indicates that localized healthcare overload did not occur randomly; rather, it was structurally rooted in the high-density and high-mobility BE context [71,72].

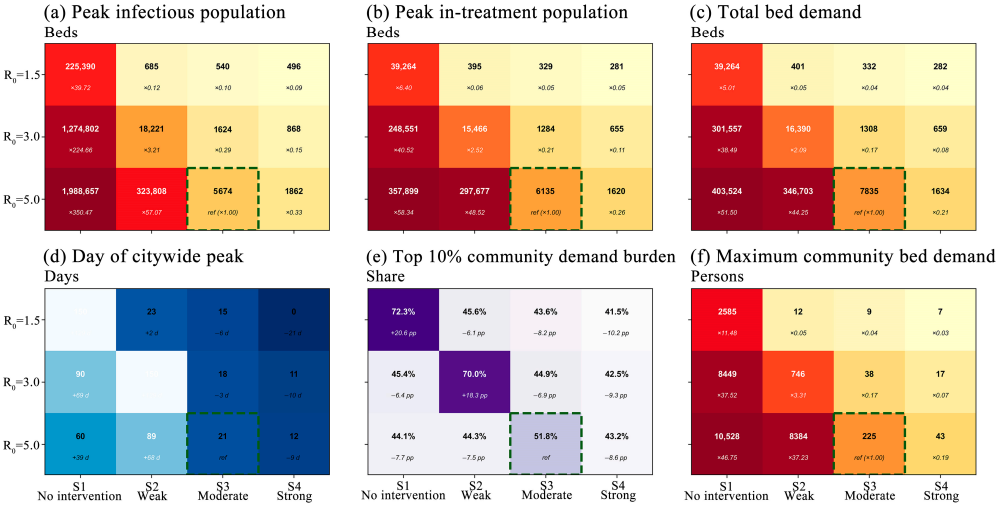


Figure 7. Scenario sensitivity matrix of key outcome indicators for emergency bed demand: (**a**) peak infectious population; (**b**) peak in-treatment population; (**c**) total bed demand; (**d**) day of citywide peak; (**e**) top 10% community demand burden; (**f**) maximum community bed demand. The green dashed boxes indicate the core scenario ($R_0 = 5.0$ with moderate intervention, S3).

To assess uncertainty in fixed parameter settings, a local sensitivity analysis using one-at-a-time ±20% perturbations was conducted. Although some parameters substantially affected bed-demand magnitude, community-level SMI rankings remained highly consistent (Spearman's $\rho \geq 0.980$), indicating robust spatial mismatch patterns across parameter perturbations (Table A1).

3.2.3. Spatial Pattern of Demand Under the Core Scenario

Based on the scenario design above, $R_0 = 5$ with moderate intervention (S3) was adopted as the core stress-test scenario for subsequent spatial diagnosis. Under this core scenario, the citywide peak of total bed demand was approximately 7835 beds and occurred around day 21. Demand was highly concentrated in the core built-up area. The top 10% of communities with the highest demand, totaling 50 communities, accounted for approximately 51.8% of citywide bed demand, and the maximum peak bed demand in a single community reached 225 beds.

Spatially, under the core scenario, peak bed demand and peak timing exhibited gradients of "high in the center and low in the periphery" (Figure 8a) and "earlier in the center and later in the periphery" (Figure 8b), respectively. The core built-up area showed high demand intensity and earlier peaks, whereas peripheral communities exhibited lower demand and delayed peaks. This pattern reflects a process in which the epidemic first erupted in the core areas with high transmission potential and then diffused outward to peripheral areas. The spatial coupling between this demand flow and the highly concentrated supply field constituted the precondition for exposing supply–demand imbalance in the release phase.

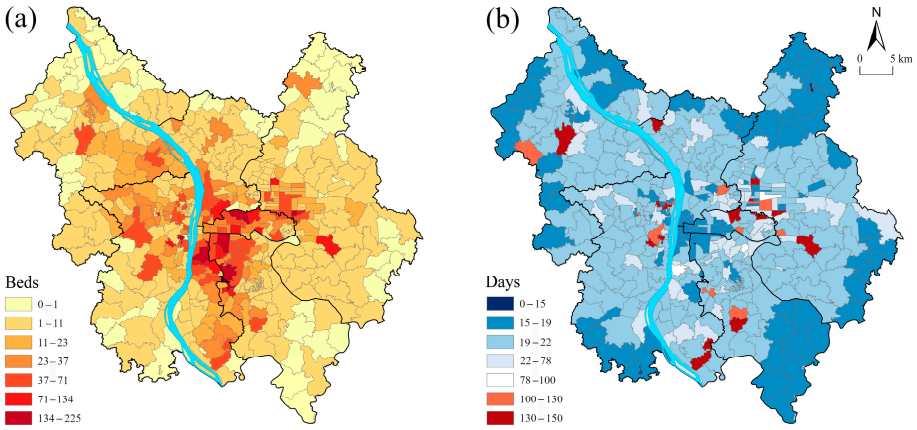


Figure 8. Spatial distribution of peak emergency bed demand and peak timing under the core scenario (R_0 = 5, S3 moderate intervention): (**a**) distribution of peak bed demand at the community scale; (**b**) distribution of peak timing of bed demand at the community scale.

3.3. Diagnosis of the Spatial Pattern of SDM

3.3.1. Spatial Pattern of Accessibility Based on 3SFCA

In the release phase of the adaptive cycle, the extent to which supply–demand imbalance is exposed depends on the spatial coupling between "demand flows" and "supply fields" under road-network and time constraints. Community weighted centroids were used as demand points, and the 18 designated hospitals were used as supply points. Emergency medical accessibility under the core scenario was measured using the 3SFCA with a 15 min threshold.

The results showed that the service coverage of existing designated hospitals displayed clear ring-like differentiation (Figure 9a). Among the 475 communities in the study area, only 104 could reach at least one designated hospital within 15 min, indicating a relatively low overall level of accessibility. Communities with medium and high accessibility values were mainly concentrated in the core built-up areas along both sides of the Xiangjiang River. Furong, Yuelu, and Kaifu districts developed relatively high response capacity because of their dense designated hospital nodes and strong road-network connectivity. In peripheral areas, accessibility generally remained at low levels due to the combined constraints of distance decay, insufficient medical resources, and poor road-network connection. The

number of accessible beds in Wangcheng District and Changsha County together accounted for less than 6% of the metropolitan total.

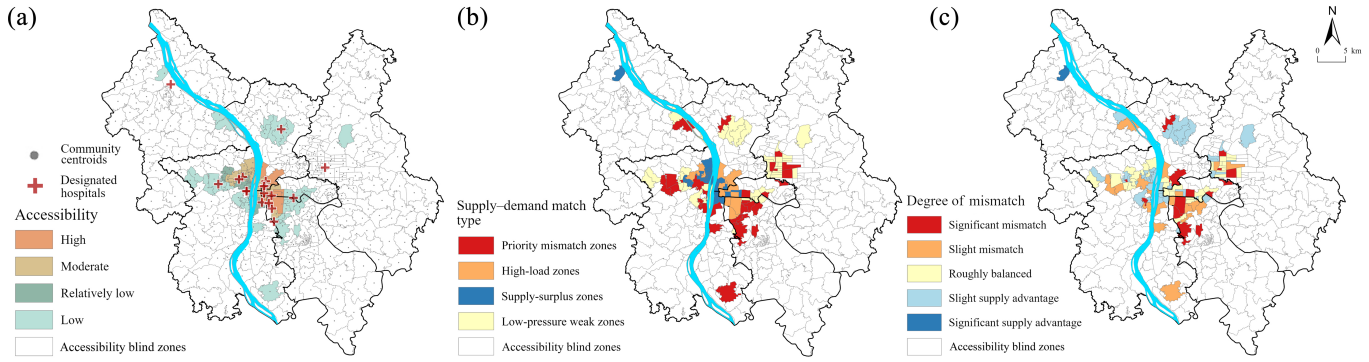


Figure 9. Spatial pattern of emergency bed SDM in the Changsha metropolitan area based on the 3SFCA–SMI framework: (**a**) emergency bed accessibility under the 15 min threshold; (**b**) SDM types based on standardized accessibility and demand; (**c**) degree of supply–demand mismatch measured by SMI.

3.3.2. Identification of Matching Types Based on Four-Quadrant Classification

A four-quadrant classification framework was constructed using standardized accessibility values on the vertical axis and standardized peak bed demand on the horizontal axis. Communities were classified into four types: priority mismatch zones with low supply and high demand, high-load zones with high supply and high demand, supply-surplus zones with high supply and low demand, and low-pressure weak zones with low supply and low demand.

Under the core scenario, emergency medical SDM in the Changsha metropolitan area no longer followed a simple pattern of "strong center and weak periphery". Instead, a composite structure emerged, characterized by "central carrying, peripheral weakness, and transitional mismatch" (Figure 9b). A total of 26 communities were identified as priority mismatch zones with high demand and low supply, accounting for 13.1% of the population (Table 7). These communities were widely distributed in the transitional zones around the core built-up areas on both sides of the Xiangjiang River and faced severe risks of systemic healthcare overload.

Table 7. Composition of community SDM types under the core scenario.

Matching Type	Demand–Supply Relationship	Number of Communities	Proportion (%)	Population	Population Proportion (%)
Priority mismatch zones	High–low	26	5.5	887,549	13.1
High-load zones	High–high	12	2.5	647,518	9.6
Supply surplus zones	Low–high	25	5.3	360,750	5.3
Low-pressure weak zones	Low–low	41	8.6	611,674	9.0
Accessibility blind zones	—	371	78.1	4,258,906	62.9
Total	—	475	100.0	6,766,397	100.0

A total of 12 communities were classified as high-load zones with high demand and high supply. These areas were mainly embedded within the core built-up area and located around large Grade-A tertiary hospitals, where high medical-resource supply and high demand overlapped. When patients from surrounding priority mismatch zones continuously concentrate in core hospitals, high-load zones may be transformed from resource-advantaged areas into system congestion areas, thereby weakening the supporting function of designated hospitals for the entire emergency medical network.

The 25 supply-surplus zones with low demand and high supply were mainly distributed around clusters of large Grade-A tertiary hospitals. These areas had relatively high accessibility but low demand and therefore could serve as supporting areas for flexible allocation and spatial coordination. However, in the absence of cross-district dispatching and bed-conversion mechanisms, an inefficient pattern may emerge in which resource idleness coexists with overload in the core areas.

Low-pressure weak zones with low demand and low supply were mainly located in the periphery of the metropolitan area. A total of 41 communities were included in this category. Although both accessibility and bed demand were low, these areas still exhibited potential vulnerability due to sparse resource distribution.

3.3.3. Quantification of Supply–Demand Spatial Mismatch Based on SMI

The SMI was further used to quantify the direction and intensity of deviation. Negative mismatch dominated both numerically and spatially, indicating prevailing demand-side pressure (Figure 9c). Under the core scenario, 21 communities showed significant negative mismatch (SMI < -0.5), among which 13 reached a severe mismatch level (SMI < -1). Spatially, these communities were distributed in patches in the core built-up area on the east bank of the Xiangjiang River and its periphery. A cross-scenario comparison showed that the number of communities with significant negative mismatch remained stable within the range of 14–29. This suggests that these mismatch target areas are robust features across the full disturbance range and can be regarded as reliable objects for planning intervention.

To assess the sensitivity of the spatial diagnosis to travel-time thresholds, the 3SFCA–SMI analysis was recalculated using 20 and 30 min thresholds while holding all other model settings constant (Table 8). The number of covered communities increased from 104 to 156 and 233, corresponding to coverage rates of 21.9%, 32.8%, and 49.1%, respectively. The SMI ranking under the 20 min threshold remained highly consistent with the 15 min baseline (Spearman's $\rho = 0.982$), whereas the correlation declined to 0.739 under the 30 min threshold, accompanied by an increase in negatively mismatched communities. This indicates that substantially expanded service catchments and cross-district competition can reconfigure spatial supply–demand relationships.

Table 8. Sensitivity analysis of SDM under alternative travel-time thresholds.

Travel-Time Threshold	Covered Communities, n, (%)	SMI < -0.5, *n*	SMI < -1, *n*	SMI Rank Correlation (ρ) with the 15 min Baseline
15 min	104 (21.9%)	21	13	1.000
20 min	156 (32.8%)	28	18	0.982
30 min	233 (49.1%)	78	37	0.739

In summary, the principal challenge of emergency medical SDM in the Changsha metropolitan area is not an aggregate shortage of beds, but a structural spatial mismatch between concentrated effective supply and spatially differentiated demand. Effective supply is highly polarized in a limited number of core nodes, whereas emergency demand is concentrated in the core built-up area and diffuses outward under disturbance. Consequently, the most pronounced mismatches occur in transitional zones where demand diffusion, supply attenuation, and travel-time constraints overlap. District-level results further show that aggregate supply sufficiency does not necessarily eliminate community-level mismatch, while Tianxin, Wangcheng, and Changsha County face clear overall supply deficits (Table 9). These findings identify priority areas for differentiated zoning-based regulation in the reorganization phase.

Table 9. Summary of SDM by district/county under the core scenario.

District	Number of Communities	Number of Blind Spots	Priority Mismatch Zones	Effective Beds	Core-Scenario Demand	Supply–Demand Ratio	Minimum SMI
Furong	23	14	3	2304	965	2.39	−2.27
Tianxin	33	25	3	303	801	0.38	−0.91
Yuelu	90	53	7	2852	1702	1.68	−4.64
Kaifu	55	44	1	2826	859	3.29	−2.56
Yuhua	63	50	7	1831	1549	1.18	−3.77
Wangcheng	83	80	0	72	429	0.17	0.66
Changsha County	128	105	5	337	1530	0.22	−2.39
Total	475	371	26	10,525	7835	1.34	—

4. Discussion

4.1. Spatial Mechanisms of Emergency Medical Supply–Demand Mismatch

Based on adaptive cycle theory, emergency medical SDM in Changsha can be interpreted as a transition from routine resource accumulation to disturbance-induced release and planning reorganization (Figure 10). Consistent with previous studies on healthcare accessibility, the findings indicate that the vulnerability of the emergency medical system is not attributable solely to an aggregate shortage of beds. Rather, it reflects the failure of resources accumulated under routine conditions to be effectively converted into timely and spatially accessible service capacity when the system is exposed to sudden disturbances [2,4]. Building on this understanding, the present study further reveals that the divergence between the static resource base and emergency response capacity is manifested through three spatially coupled processes: the hierarchical concentration of effective emergency bed capacity, spatially differentiated surges in demand, and travel-time constraints imposed by the road network.

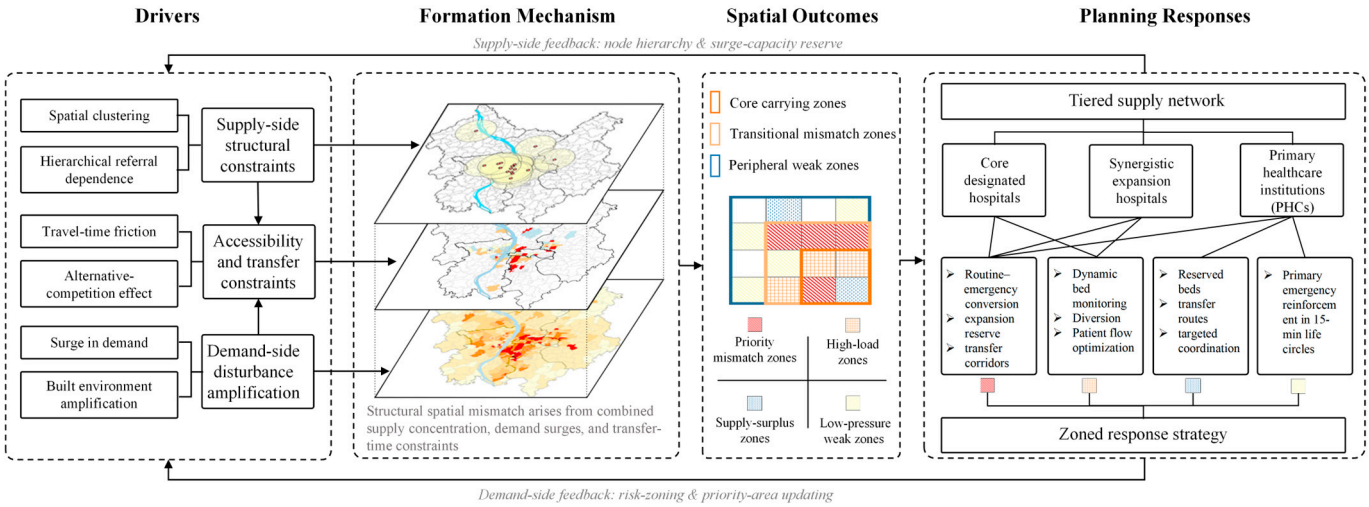


Figure 10. Supply–demand coupling and feedback mechanism for emergency medical planning in Changsha.

On the supply side, the long-term accumulation of medical resources along administrative hierarchies and gradients of urban development intensity has produced a spatial structure dominated by the urban core and higher-tier hospitals. On the demand side, PHEs do not amplify medical demand uniformly in proportion to the permanent resident population. Instead, heterogeneous demand shocks emerge through the combined effects of the built environment, population mobility, the distribution of vulnerable groups, and

variations in governance intervention. This finding is consistent with spatial epidemiological research showing that epidemic transmission is strongly shaped by spatial heterogeneity and interregional interactions. However, the present study does not simply reproduce the conventional "strong center–weak periphery" pattern commonly identified in routine healthcare accessibility studies [73,74]. Once heterogeneous demand shocks interact with an existing core-concentrated supply structure under transfer-time constraints, the spatial pattern of risk is further reorganized into a composite structure comprising core carrying zones, transitional mismatch zones, and peripheral weak zones. Notably, the weakest points of emergency medical resilience are not necessarily located in the most remote communities. Instead, they tend to emerge in transitional areas surrounding the core built-up area [75]. These areas lie simultaneously at the diffusion frontier of high-intensity demand and the decay boundary of timely access to higher-tier medical resources concentrated in the urban core. The spatial superposition of demand growth, supply attenuation, and transfer-time constraints therefore generates a more structurally embedded form of emergency vulnerability.

The scenario comparison further shows that several priority mismatch communities remained stable across disturbance settings. These communities should therefore be treated as robust targets for planning intervention, rather than as accidental outcomes under a single epidemic scenario. This finding supports a shift from passive gap filling after demand surges to proactive reservation, conversion, and transfer organization under routine–emergency dual-use planning.

4.2. Planning Responses: Tiered Supply Network and Zoned Strategy

Planning interventions should move beyond homogeneous capacity expansion based on aggregate administrative-unit indicators and address both supply-network organization and spatially differentiated demand risks. Accordingly, the mismatch diagnosis is translated into two complementary responses: a tiered supply network and a zoned response strategy (Figure 10). The former addresses the supply-side question of where emergency capacity can be generated and how it should be organized, whereas the latter addresses the demand-side question of where limited resources should be prioritized and what types of intervention should be implemented. Together, they establish a "node–network–area" linkage within the emergency medical system and support a cyclical planning process of routine accumulation–disturbance-induced release–mismatch diagnosis–system reorganization–reaccumulation.

The tiered supply network represents the supply-side feedback from point-based resources to networked surge capacity. Major designated hospitals should serve as core critical-care nodes; secondary and higher-level hospitals with conversion potential should be incorporated as synergistic expansion nodes; and PHCIs should function as early-warning, triage, and referral interfaces embedded in 15 min community life circles [76]. This structure can enhance hierarchy, redundancy, and convertibility in the emergency medical network.

The zoned response strategy represents a demand-side feedback mechanism that translates mismatch diagnosis into prioritized spatial intervention. For priority mismatch zones characterized by high demand and low effective supply, the principal challenge is the direct gap between peak demand and timely service capacity. Convertible beds should therefore be reserved in advance, cross-district transfer routes should be predefined, and targeted support arrangements should be established with nearby supply-surplus nodes or synergistic expansion hospitals. For core carrying zones characterized by high demand and high supply, the existing resource base is relatively strong, but sustained demand shocks may transform high load into systemic overload. These areas should therefore prioritize dy-

namic bed monitoring, optimization of internal patient flows, and predefined cross-district diversion before early-warning thresholds are reached. In supply-surplus zones, planning should avoid further expansion of fixed capacity and instead incorporate spare capacity into regional coordination networks through predefined dispatching arrangements. Low-pressure weak zones, characterized by both low demand and low supply, should maintain essential baseline emergency capacity and reinforce primary-level response functions to prevent new mismatches from emerging when demand rises unexpectedly. For accessibility blind zones located beyond the 15 min service threshold, priority should be given to improving transfer connectivity, while the need for additional primary-level emergency nodes or coordinated transfer facilities should be assessed according to population size and risk levels.

4.3. Methodological Integration and Contributions

The methodological contribution of this study does not lie in proposing a new standalone model. Rather, grounded in adaptive cycle theory, it establishes an explicit information-transfer mechanism linking epidemic disturbance simulation, spatial supply–demand matching, and mismatch diagnosis. In conventional healthcare accessibility studies, demand is commonly treated as an exogenous and relatively static input, such as the permanent resident population or the estimated number of potential patients at a given time point. Although infectious-disease dynamic models can characterize epidemic evolution over time, they often terminate at predictions of infection magnitude, peak timing, or intervention effects, and less frequently address how dynamically generated healthcare demand is translated into spatial competition, localized overload, and accessibility mismatch within an actual healthcare facility network. In this study, communities are used as the common spatial unit, and the peak emergency bed demand simulated by the SEIQRDP-SG model under different transmission and intervention scenarios is directly incorporated as the demand input to the 3SFCA model. This demand is then jointly evaluated against the effective emergency supply of designated hospitals, road-network travel times, and facility competition. The SMI is subsequently used to identify the direction and intensity of spatial mismatch. Epidemic evolution is therefore not treated as an independent background scenario; instead, changes in demand generated by the disturbance process are directly transmitted into hospital supply–demand ratios, community-level accessibility, and spatial mismatch patterns.

The study extends existing research in three respects. First, compared with healthcare accessibility studies based on 2SFCA, 3SFCA, and their variants, population demand is not treated as a fixed input but is explicitly linked to the evolution of public health disturbances, allowing accessibility outcomes to vary with transmission intensity and intervention strength. Second, compared with SEIR-type dynamic models primarily designed for epidemic forecasting and intervention assessment, the present framework translates disease-transmission outcomes into spatially explicit emergency bed pressure with direct implications for facility demand, and subsequently evaluates whether such demand can be absorbed by the healthcare service network. Third, compared with existing static–dynamic frameworks for urban health resilience, this study operates at a finer spatial scale by translating city-level disturbances into specific community–hospital supply–demand relationships, thereby identifying localized mismatches and potential systemic overload nodes that aggregate resource indicators may fail to reveal.

5. Conclusions

Taking the Changsha metropolitan area as the empirical case, this study developed a dynamic framework for emergency medical facility SDM based on adaptive cycle theory.

By integrating the SEIQRDP-SG model, 3SFCA, and SMI, the study identified how routine medical-resource accumulation is transformed into emergency spatial mismatch under public health disturbances. The findings show that the key constraint on emergency medical resilience is not aggregate bed shortage alone, but a structural mismatch jointly shaped by effective supply, dynamic demand, and transfer-time constraints.

Three main conclusions can be drawn. First, effective emergency bed capacity is highly concentrated in higher-tier designated hospitals in the core urban area, whereas peripheral districts have markedly weaker supply. Second, under the core scenario of $R_0 = 5$ with moderate intervention, emergency bed demand peaks at approximately 7835 beds around day 21 and exhibits strong spatial heterogeneity, with high-demand communities concentrated in the core built-up area and adjacent expansion zones. Third, the coupling of supply polarization and demand diffusion produces a composite structure of core carrying zones, transitional mismatch zones, peripheral weak zones, and accessibility blind zones. Priority mismatch zones represent robust intervention targets because they remain exposed across multiple disturbance scenarios.

Based on these findings, emergency medical planning should be adjusted simultaneously from the perspectives of supply-network organization and spatially differentiated response. On the supply side, a tiered emergency supply network should be established by integrating core designated hospitals, synergistic expansion hospitals, and PHCIs, thereby transforming routine medical resources into an emergency capacity system that can be activated hierarchically, converted flexibly, and coordinated across districts. On the demand side, reserved beds, transfer corridors, dynamic monitoring, cross-district diversion, surplus-capacity dispatching, and primary-level response capacity should be allocated according to different mismatch types. Together, these measures form a "node–network–area" spatial response mechanism that enables limited emergency resources to be directed preferentially toward high-risk areas and locations with persistent mismatch.

Several limitations should nevertheless be acknowledged. First, the study primarily uses effective emergency bed capacity as the core supply indicator and does not fully incorporate specialized treatment capacity, medical staffing, or emergency material reserves. Second, some model parameters are scenario-based and require further calibration against epidemiological surveillance data and empirical healthcare utilization records. Third, the uniform 15 min threshold represents modeled road-network transfer time rather than the complete prehospital emergency-care process. The analysis does not explicitly incorporate emergency-call processing, ambulance availability, dispatch and on-scene delays, triage, prehospital stabilization, real-time traffic congestion, hospital handover, or differences in patient severity. Fourth, the use of community-level spatial units may be affected by the modifiable areal unit problem (MAUP), and cross-jurisdictional healthcare flows have not yet been incorporated. Future research could integrate dynamic traffic and healthcare-utilization data to improve spatiotemporal accuracy, employ finer-scale population data to test model robustness, and extend the framework to the metropolitan-region scale to incorporate cross-jurisdictional coordination and emergency resource sharing.

Author Contributions: Conceptualization, Ying Zhong and Sheng Jiao; methodology, Ying Zhong and Sheng Jiao; software, Ying Zhong; validation, Ying Zhong, Qingqing Zhang and Yizhe Ying; formal analysis, Ying Zhong; investigation, Ying Zhong, Qingqing Zhang and Yizhe Ying; resources, Sheng Jiao and Qingqing Zhang; data curation, Ying Zhong and Yizhe Ying; writing—original draft preparation, Ying Zhong; writing—review and editing, Sheng Jiao, Qingqing Zhang and Yizhe Ying; visualization, Ying Zhong and Yizhe Ying; supervision, Sheng Jiao; project administration, Sheng Jiao; funding acquisition, Sheng Jiao. All authors have read and agreed to the published version of the manuscript.

Funding: This research was funded by the National Key Research and Development Program of China, grant number 2024YFC3808504); the Changsha Municipal Bureau of Natural Resources, through the project "Special Planning Research on 'Dual-Use' Public Infrastructure for Routine and Emergency Conditions in Changsha", project number C13010000; and the Department of Natural Resources of Hunan Province, through the project "Optimization Research on Territorial Spatial Special Planning in Hunan Province under the Background of 'Dual-Use' for Routine and Emergency Conditions", project number 815202402696.

Data Availability Statement: The publicly available datasets used in this study are described in Section 2, including administrative boundaries, road networks, population data, POI data, and other geospatial datasets. The derived datasets, model outputs, and analytical results generated during the current study are available from the corresponding author upon reasonable request. Some hospital-related planning materials and construction-plan data are not publicly available due to data confidentiality and project restrictions.

Conflicts of Interest: The authors declare no conflicts of interest. The funders had no role in the design of the study; in the collection, analyses, or interpretation of data; in the writing of the manuscript; or in the decision to publish the results.

Appendix A

To further assess parameter uncertainty, a one-at-a-time local sensitivity analysis was conducted under the core scenario by perturbing key epidemiological and spatial heterogeneity parameters by ±20%. Because the model is deterministic and its parameters were specified from literature-supported scenarios rather than statistically estimated from repeated observations, no sampling distribution was available from which conventional confidence intervals could be derived. Uncertainty was therefore characterized by scenario variation, parameter perturbation, and rank-stability tests. The results show that peak bed demand was most sensitive to γ, followed by σ and α, whereas κ and η had relatively limited effects. Across all perturbations, total bed demand ranged from 4762 to 12,738 beds, corresponding to a supply–demand ratio of 0.83–2.21. Despite these variations in demand magnitude, the SMI rankings remained highly consistent with the baseline results (Spearman's $\rho \geq 0.980$), indicating strong robustness of the spatial mismatch pattern (Table A1). Accordingly, the baseline supply–demand ratio of 1.34 should be interpreted as a scenario-specific output rather than a population estimate with a sampling-based confidence interval.

Table A1. Local sensitivity analysis of key SEIQRDP-SG model outputs under ±20% parameter perturbations.

Parameter Category	Parameter	Change in Peak Bed Demand		Supply–Demand Ratio Range	Minimum SMI Rank Correlation
		−20%	+20%		
Epidemiological	σ	−27.4%	28.9%	1.04–1.85	0.997
	γ	−39.2%	62.6%	0.83–2.21	0.980
	λ	18.5%	−13.4%	1.13–1.55	0.998
	κ	0.8%	−0.8%	1.33–1.35	1.000
Spatial/Governance	α	−20.7%	28.5%	1.05–1.69	0.991
	η	−6.3%	10.6%	1.21–1.43	0.980

References

1. Legido-Quigley, H.; Mateos-García, J.T.; Campos, V.R.; Gea-Sánchez, M.; Muntaner, C.; McKee, M. The Resilience of the Spanish Health System against the COVID-19 Pandemic. *Lancet Public Health* **2020**, *5*, e251–e252. [CrossRef] [PubMed]
2. Park, J.; Michels, A.; Lyu, F.; Han, S.Y.; Wang, S. Daily Changes in Spatial Accessibility to ICU Beds and Their Relationship with the Case-Fatality Ratio of COVID-19 in the State of Texas, USA. *Appl. Geogr.* **2023**, *154*, 102929. [CrossRef] [PubMed]

3. Alisan, O.; Ulak, M.B.; Ozguven, E.E.; Horner, M.W. Location Selection of Field Hospitals amid COVID-19 Considering Effectiveness and Fairness: A Case Study of Florida. *Int. J. Disaster Risk Reduct.* **2023**, *93*, 103794. [CrossRef] [PubMed]
4. Chen, M.; Peng, M.; Li, B.; Cai, Z.; Li, R. Static–Dynamic Analytical Framework for Urban Health Resilience Evaluation and Influencing Factor Exploration from the Perspective of Public Health Emergencies—Case Study of 61 Cities in Mainland China. *ISPRS Int. J. Geo-Inf.* **2025**, *14*, 176. [CrossRef]
5. Rezapour, S.; Farahani, R.Z.; Tajik, N. Impact of Timing in Post-Warning Prepositioning Decisions on Performance Measures of Disaster Management: A Real-Life Application. *Eur. J. Oper. Res.* **2021**, *293*, 312–335. [CrossRef]
6. Klein, B.; LaRock, T.; McCabe, S.; Torres, L.; Friedland, L.; Kos, M.; Privitera, F.; Lake, B.; Kraemer, M.U.G.; Brownstein, J.S.; et al. Characterizing Collective Physical Distancing in the U.S. during the First Nine Months of the COVID-19 Pandemic. *PLoS Digit. Health* **2024**, *3*, e0000430. [CrossRef] [PubMed]
7. General Office of the State Council of the People's Republic of China. *Guiding Opinions on Actively and Steadily Advancing the Construction of "Dual-Use" Public Infrastructure in Mega-Cities*; State Council: Beijing, China, 2023. Available online: https://www.gov.cn (accessed on 10 January 2026). (In Chinese)
8. Fang, D.; Pan, S.; Li, Z.; Yuan, T.; Jiang, B.; Gan, D.; Sheng, B.; Han, J.; Wang, T.; Liu, Z. Large-Scale Public Venues as Medical Emergency Sites in Disasters: Lessons from COVID-19 and the Use of Fangcang Shelter Hospitals in Wuhan, China. *BMJ Glob. Health* **2020**, *5*, e002815. [CrossRef] [PubMed]
9. Chen, S.; Zhang, Z.; Yang, J.; Wang, J.; Zhai, X.; Bärnighausen, T.; Wang, C. Fangcang Shelter Hospitals: A Novel Concept for Responding to Public Health Emergencies. *Lancet* **2020**, *395*, 1305–1314. [CrossRef] [PubMed]
10. Li, Q.; Wang, L.; Wang, B.; Lu, H. The COVID-19-Designated Hospitals in China: Preparing for Public Health Emergencies. *Emerg. Microbes Infect.* **2021**, *10*, 998–1001. [CrossRef] [PubMed]
11. Shen, X. Accessibility calculation and equality evaluation of medical facilities for COVID-19 pandemic treatment: A case study of the wuhan metropolitan development zone. *PLoS ONE* **2022**, *17*, e0272458. [CrossRef] [PubMed]
12. Ye, Y.; Huang, L.; Wang, J.; Chuang, Y.-C.; Pan, L. Patient Allocation Method in Major Epidemics under the Situation of Hierarchical Diagnosis and Treatment. *BMC Med. Inf. Decis. Mak.* **2022**, *22*, 331. [CrossRef] [PubMed]
13. Chen, Y.; Xu, L.; Shi, L. Spatial Adaptive Measures of the Emergency Departments in Response to the COVID-19 Surge—A Case Study of the Central City Area of Shanghai, China. *HERD* **2026**, *19*, 254–276. [CrossRef] [PubMed]
14. Pereira, R.H.M.; Braga, C.K.V.; Servo, L.M.; Serra, B.; Amaral, P.; Gouveia, N.; Paez, A. Geographic Access to COVID-19 Healthcare in Brazil Using a Balanced Float Catchment Area Approach. *Soc. Sci. Med.* **2021**, *273*, 113773. [CrossRef] [PubMed]
15. Jiao, W.; Huang, W.; Fan, H. Evaluating Spatial Accessibility to Healthcare Services from the Lens of Emergency Hospital Visits Based on Floating Car Data. *Int. J. Digit. Earth* **2022**, *15*, 108–133. [CrossRef]
16. Qiang, H.; Xie, X.; Wang, H.; Xiong, W. Spatial Mismatch and Hierarchical Optimization of Healthcare Facilities: A Multi-Source Geospatial Analysis of Accessibility and Supply-Demand Dynamics. *Int. J. Health Geogr.* **2025**, *25*, 16. [CrossRef] [PubMed]
17. Guagliardo, M.F. Spatial Accessibility of Primary Care: Concepts, Methods and Challenges. *Int. J. Health Geogr.* **2004**, *3*, 3. [CrossRef] [PubMed]
18. Luo, W.; Wang, F.H. Measures of Spatial Accessibility to Health Care in a GIS Environment: Synthesis and a Case Study in the Chicago Region. *Environ. Plan. B-Plan. Des.* **2003**, *30*, 865–884. [CrossRef] [PubMed]
19. Luo, W.; Qi, Y. An Enhanced Two-Step Floating Catchment Area (E2SFCA) Method for Measuring Spatial Accessibility to Primary Care Physicians. *Health Place* **2009**, *15*, 1100–1107. [CrossRef] [PubMed]
20. Dai, D. Black Residential Segregation, Disparities in Spatial Access to Health Care Facilities, and Late-Stage Breast Cancer Diagnosis in Metropolitan Detroit. *Health Place* **2010**, *16*, 1038–1052. [CrossRef] [PubMed]
21. Luo, W.; Whippo, T. Variable Catchment Sizes for the Two-Step Floating Catchment Area (2SFCA) Method. *Health Place* **2012**, *18*, 789–795. [CrossRef] [PubMed]
22. McGrail, M.R.; Humphreys, J.S. Measuring Spatial Accessibility to Primary Health Care Services: Utilising Dynamic Catchment Sizes. *Appl. Geogr.* **2014**, *54*, 182–188. [CrossRef]
23. Chen, B.Y.; Cheng, X.-P.; Kwan, M.-P.; Schwanen, T. Evaluating Spatial Accessibility to Healthcare Services under Travel Time Uncertainty: A Reliability-Based Floating Catchment Area Approach. *J. Transp. Geogr.* **2020**, *87*, 102794. [CrossRef]
24. Huang, Z.; Sun, Y. Assessing Emergency Medical Services (EMS) Accessibility before and after Road Pricing: A Dynamic 2SFCA Approach. *J. Transp. Geogr.* **2026**, *130*, 104489. [CrossRef]
25. Delamater, P.L. Spatial Accessibility in Suboptimally Configured Health Care Systems: A Modified Two-Step Floating Catchment Area (M2SFCA) Metric. *Health Place* **2013**, *24*, 30–43. [CrossRef] [PubMed]
26. Wan, N.; Zou, B.; Sternberg, T. A Three-Step Floating Catchment Area Method for Analyzing Spatial Access to Health Services. *Int. J. Geogr. Inf. Sci.* **2012**, *26*, 1073–1089. [CrossRef]
27. Luo, J. Integrating the Huff Model and Floating Catchment Area Methods to Analyze Spatial Access to Healthcare Services. *Trans. GIS* **2014**, *18*, 436–448. [CrossRef]

28. Subal, J.; Paal, P.; Krisp, J.M. Quantifying Spatial Accessibility of General Practitioners by Applying a Modified Huff Three-Step Floating Catchment Area (MH3SFCA) Method. *Int. J. Health Geogr.* **2021**, *20*, 9. [CrossRef] [PubMed]
29. Kim, K.; Ghorbanzadeh, M.; Horner, M.W.; Ozguven, E.E. Identifying Areas of Potential Critical Healthcare Shortages: A Case Study of Spatial Accessibility to ICU Beds during the COVID-19 Pandemic in Florida. *Transp. Policy* **2021**, *110*, 478–486. [CrossRef] [PubMed]
30. Chen, Y.; Jia, S.; Xu, Q.; Xiao, Z.; Zhang, S. Measuring the Dynamic Accessibility to COVID-19 Testing Sites in the 15-Min City: A Focus on Service Congestion and Mobility Difference. *J. Transp. Geogr.* **2023**, *111*, 103670. [CrossRef]
31. Hou, X.; Gao, S.; Li, Q.; Kang, Y.; Chen, N.; Chen, K.; Rao, J.; Ellenberg, J.S.; Patz, J.A. Intracounty Modeling of COVID-19 Infection with Human Mobility: Assessing Spatial Heterogeneity with Business Traffic, Age, and Race. *Proc. Natl. Acad. Sci. USA* **2021**, *118*, e2020524118. [CrossRef] [PubMed]
32. Kraemer, M.U.G.; Yang, C.-H.; Gutierrez, B.; Wu, C.-H.; Klein, B.; Pigott, D.M.; Covid, O.; Hanage, W.P.; Brownstein, J.S.; Layan, M.; et al. The Effect of Human Mobility and Control Measures on the COVID-19 Epidemic in China. *Science* **2020**, *368*, 493–497. [CrossRef] [PubMed]
33. Chang, S.; Pierson, E.; Koh, P.W.; Gerardin, J.; Redbird, B.; Grusky, D.; Leskovec, J. Mobility Network Models of COVID-19 Explain Inequities and Inform Reopening. *Nature* **2021**, *589*, 82–87. [CrossRef] [PubMed]
34. Holling, C.S. Understanding the Complexity of Economic, Ecological, and Social Systems. *Ecosystems* **2001**, *4*, 390–405. [CrossRef]
35. Sharifi, A.; Khavarian-Garmsir, A.R. The COVID-19 Pandemic: Impacts on Cities and Major Lessons for Urban Planning, Design, and Management. *Sci. Total Environ.* **2020**, *749*, 142391. [CrossRef] [PubMed]
36. Haldane, V.; De Foo, C.; Abdalla, S.M.; Jung, A.-S.; Tan, M.; Wu, S.; Chua, A.; Verma, M.; Shrestha, P.; Singh, S.; et al. Health Systems Resilience in Managing the COVID-19 Pandemic: Lessons from 28 Countries. *Nat. Med.* **2021**, *27*, 964–980. [CrossRef] [PubMed]
37. Khalil, M.; Ravaghi, H.; Samhouri, D.; Abo, J.; Ali, A.; Sakr, H.; Camacho, A. What Is "Hospital Resilience"? A Scoping Review on Conceptualization, Operationalization, and Evaluation. *Front. Public Health* **2022**, *10*, 1009400. [CrossRef] [PubMed]
38. Kruk, M.E.; Myers, M.; Varpilah, S.T.; Dahn, B.T. What Is a Resilient Health System? Lessons from Ebola. *Lancet* **2015**, *385*, 1910–1912. [CrossRef] [PubMed]
39. Arsenault, C.; Gage, A.; Kim, M.K.; Kapoor, N.R.; Akweongo, P.; Amponsah, F.; Aryal, A.; Asai, D.; Awoonor-Williams, J.K.; Ayele, W.; et al. COVID-19 and Resilience of Healthcare Systems in Ten Countries. *Nat. Med.* **2022**, *28*, 1314–1324. [CrossRef] [PubMed]
40. Witter, S.; Thomas, S.; Topp, S.M.; Barasa, E.; Chopra, M.; Cobos, D.; Blanchet, K.; Teddy, G.; Atun, R.; Ager, A. Health System Resilience: A Critical Review and Reconceptualisation. *Lancet Glob. Health* **2023**, *11*, E1454–E1458. [CrossRef] [PubMed]
41. Saulnier, D.; Duchenko, A.; Ottilie-Kovelman, S.; Tediosi, F.; Blanchet, K. Re-Evaluating Our Knowledge of Health System Resilience during COVID-19: Lessons from the First Two Years of the Pandemic. *Int. J. Health Policy Manag.* **2023**, *12*, 6659. [CrossRef] [PubMed]
42. Chen, Y.; Xu, C.; Ge, Y.; Zhang, X.; Zhou, Y. A 100 m Gridded Population Dataset of China's Seventh Census Using Ensemble Learning and Big Geospatial Data. *Earth Syst. Sci. Data* **2024**, *16*, 3705–3718. [CrossRef]
43. Rosenback, R.; Eriksson, K.M. COVID-19 Healthcare Success or Failure? Crisis Management Explained by Dynamic Capabilities. *BMC Health Serv. Res.* **2024**, *24*, 759. [CrossRef] [PubMed]
44. Zhong, S.; Clark, M.; Hou, X.-Y.; Zang, Y.; FitzGerald, G. Development of Key Indicators of Hospital Resilience: A Modified Delphi Study. *J. Health Serv. Res. Policy* **2015**, *20*, 74–82. [CrossRef] [PubMed]
45. Yu, T.; Lin, T.; Li, Q. Study on the Supply and Demand of Urban Emergency Medical Treatment Spaces under Public Health Emergencies. *Urban Rural Plan.* **2022**, *6*, 115–124. Available online: https://chn.oversea.cnki.net/kcms/detail/detail.aspx?dbcode=CJFD&filename=GHCX202206013 (accessed on 29 July 2026). (In Chinese)
46. Hatami, F.; Chen, S.; Paul, R.; Thill, J.-C. Simulating and forecasting the COVID-19 spread in a U.S. metropolitan region with a spatial SEIR model. *Int. J. Environ. Res. Public Health* **2022**, *19*, 15771. [CrossRef] [PubMed]
47. Chen, J.; Sun, Z.; Wu, Y.; Hu, G.; Wen, Y. Scale-Specific Effects of Urban Landscape Pattern on the COVID-19 Epidemic in Hangzhou, China. *Landsc. Ecol.* **2024**, *39*, 192. [CrossRef]
48. Thornton, S.R.; Acquesta, E.C.S.; Finley, P.D.; Haider, M.A. A Multi-Region SEIR Model Incorporating Inter-County Mobility and Time-Dependent Transmission Dynamics: Application to COVID-19 Disease Outbreak Data in North Carolina. *Bull. Math. Biol.* **2026**, *88*, 39. [CrossRef] [PubMed]
49. Chishtie, F.A.; Drozd, J.; Li, X.; Benterki, A.; Valluri, S.R. A Robust Compartmental Modeling Framework for Infectious Disease Monitoring and Analysis via Fractional Differential Equations. *Epidemics* **2026**, *54*, 100887. [CrossRef] [PubMed]
50. Liu, Y.; Gayle, A.A.; Wilder-Smith, A.; Rocklöv, J. The Reproductive Number of COVID-19 Is Higher Compared to SARS Coronavirus. *J. Travel Med.* **2020**, *27*, taaa021. [CrossRef] [PubMed]
51. Sanche, S.; Lin, Y.T.; Xu, C.; Romero-Severson, E.; Hengartner, N.; Ke, R. High Contagiousness and Rapid Spread of Severe Acute Respiratory Syndrome Coronavirus 2. *Emerg. Infect. Dis.* **2020**, *26*, 1470–1477. [CrossRef] [PubMed]
52. Li, Q.; Guan, X.; Wu, P.; Wang, X.; Zhou, L.; Tong, Y.; Ren, R.; Leung, K.S.M.; Lau, E.H.Y.; Wong, J.Y.; et al. Early Transmission Dynamics in Wuhan, China, of Novel Coronavirus-Infected Pneumonia. *N. Engl. J. Med.* **2020**, *382*, 1199–1207. [CrossRef] [PubMed]

53. Forslid, R.; Herzing, M. Assessing the Consequences of Quarantines during a Pandemic. *Eur. J. Health Econ.* **2021**, *22*, 1115–1128. [CrossRef] [PubMed]
54. Zhao, W.; Sun, Y.; Li, Y.; Guan, W. Prediction of COVID-19 Data Using Hybrid Modeling Approaches. *Front. Public Health* **2022**, *10*, 923978. [CrossRef] [PubMed]
55. Zhou, F.; Yu, T.; Du, R.; Fan, G.; Liu, Y.; Liu, Z.; Xiang, J.; Wang, Y.; Song, B.; Gu, X.; et al. Clinical Course and Risk Factors for Mortality of Adult Inpatients with COVID-19 in Wuhan, China: A Retrospective Cohort Study. *Lancet* **2020**, *395*, 1054–1062. [CrossRef] [PubMed]
56. Rees, E.M.; Nightingale, E.S.; Jafari, Y.; Waterlow, N.R.; Clifford, S.; Pearson, C.A.B.; Jombart, T.; Procter, S.R.; Knight, G.M. COVID-19 Length of Hospital Stay: A Systematic Review and Data Synthesis. *BMC Med.* **2020**, *18*, 270. [CrossRef] [PubMed]
57. Verity, R.; Okell, L.C.; Dorigatti, I.; Winskill, P.; Whittaker, C.; Imai, N.; Cuomo-Dannenburg, G.; Thompson, H.; Walker, P.G.T.; Fu, H.; et al. Estimates of the Severity of Coronavirus Disease 2019: A Model-Based Analysis. *Lancet Infect. Dis.* **2020**, *20*, 669–677. [CrossRef] [PubMed]
58. Guo, W.; Wang, J.; Liu, X.; Pan, Z.; Zhuang, R.; Li, C.; Tang, H. Towards Resilient Communities: Evaluating the Nonlinear Impact of the Built Environment on COVID-19 Transmission Risk in Residential Areas. *Build. Environ.* **2025**, *267*, 112289. [CrossRef]
59. Lakes, T.; Schmitz, T.; Fueller, H. Pathogenic Built Environment? Reflections on Modeling Spatial Determinants of Health in Urban Settings Considering the Example of COVID-19 Studies. *Front. Public Health* **2025**, *13*, 1502897. [CrossRef] [PubMed]
60. Zhao, L.; Wu, X. Multi-Level Urban Environments and Population Mobility Shape Urban Epidemic Dynamics: A Study in Beijing. *Sustain. Cities Soc.* **2026**, *144*, 107394. [CrossRef]
61. Hsiang, S.; Allen, D.; Annan-Phan, S.; Bell, K.; Bolliger, I.; Chong, T.; Druckenmiller, H.; Huang, L.Y.; Hultgren, A.; Krasovich, E.; et al. The Effect of Large-Scale Anti-Contagion Policies on the COVID-19 Pandemic. *Nature* **2020**, *584*, 262–267. [CrossRef] [PubMed]
62. Zhang, D.; Yang, W.; Wen, W.; Peng, L.; Zhuge, C.; Hong, L. A Data-Driven Analysis on the Mediation Effect of Compartment Models between Control Measures and COVID-19 Epidemics. *Heliyon* **2024**, *10*, e33850. [CrossRef] [PubMed]
63. Kociurzynski, R.; D'Ambrosio, A.; Papathanassopoulos, A.; Buerkin, F.; Hertweck, S.; Eichel, V.M.; Heininger, A.; Liese, J.; Mutters, N.T.; Peter, S.; et al. Forecasting Local Hospital Bed Demand for COVID-19 Using on-Request Simulations. *Sci. Rep.* **2023**, *13*, 21321. [CrossRef] [PubMed]
64. Mendes, J.M.; Coelho, P.S. Addressing Hospitalisations with Non-Error-Free Data by Generalised SEIR Modelling of COVID-19 Pandemic. *Sci. Rep.* **2021**, *11*, 19617. [CrossRef] [PubMed]
65. Liu, Y.; Rockloev, J. The Effective Reproductive Number of the Omicron Variant of SARS-CoV-2 Is Several Times Relative to Delta. *J. Travel Med.* **2022**, *29*, taac037. [CrossRef] [PubMed]
66. Cai, J.; Deng, X.; Yang, J.; Sun, K.; Liu, H.; Chen, Z.; Peng, C.; Chen, X.; Wu, Q.; Zou, J.; et al. Modeling Transmission of SARS-CoV-2 Omicron in China. *Nat. Med.* **2022**, *28*, 1468–1475. [CrossRef]
67. Park, J.; Lyu, F.; Michels, A.; Zhang, I.; Wang, S. Customized Decision-Making Support per Location's Characteristics of Spatial Accessibility: A Case Study of Emergency Healthcare in New York City. *Comput. Environ. Urban Syst.* **2026**, *128*, 102458. [CrossRef]
68. He, Y.; Chen, L.; Wei, B.; Guang, X.; He, R.; Xue, H.; He, X.; Zhang, N.; Zhang, J.; Zheng, J.; et al. Evaluation and optimization of emergency medical services accessibility based on real-world emergency calls in metropolitan China. *Comput. Urban Sci.* **2025**, *5*, 45. [CrossRef]
69. Zhou, Y.; Zhao, K.; Han, J.; Zhao, S.; Cao, J. Geographical Pattern Evolution of Health Resources in China: Spatio-Temporal Dynamics and Spatial Mismatch. *Trop. Med. Infect. Dis.* **2022**, *7*, 292. [CrossRef] [PubMed]
70. Lin, S.; Qin, S.; Peng, L.; Sun, X.; Dou, X. Assessing Geographic Barriers to Access Long-Term Services and Supports in Chengdu, China: A Spatial Accessibility Analysis. *Sustainability* **2025**, *17*, 3222. [CrossRef]
71. Hu, Y.; Wang, S.; Liang, H. Mastering the Twin–Game: Hierarchical Reinforcement Learning in a Digital Twin Sandbox for Adaptive Urban Healthcare Optimization—A Case Study of Wuhan. *ISPRS Int. J. Geo-Inf.* **2026**, *15*, 273. [CrossRef]
72. Wang, L.; Hu, Z.; Zhou, K.; Kwan, M.-P. Identifying Spatial Heterogeneity of COVID-19 Transmission Clusters and Their Built-Environment Features at the Neighbourhood Scale. *Health Place* **2023**, *84*, 103130. [CrossRef] [PubMed]
73. Xing, J.; Ng, S.T. Analyzing spatiotemporal accessibility patterns to tertiary healthcare services by integrating total travel cost into an improved E3SFCA method in changsha, China. *Cities* **2022**, *122*, 103541. [CrossRef]
74. Mahmut, M.; Yin, P.; Peng, B.; Wu, J.; Wang, T.; Yuan, S.; Zhang, Y. Examining spatial accessibility and equity of public hospitals for older adults in songjiang district, shanghai. *ISPRS Int. J. Geo-Inf.* **2024**, *13*, 403. [CrossRef]
75. Liu, C.; Su, H.; Leng, H.; Chen, W. Spatial and social equity in access to emergency service facilities—An opportunity–outcome perspective. *ISPRS Int. J. Geo-Inf.* **2026**, *15*, 95. [CrossRef]
76. Wang, B.; Sun, M. Optimizing the Layout of Primary Healthcare Facilities in Harbin's Main Urban Area, China: A Resilience Perspective. *Sustainability* **2025**, *17*, 8706. [CrossRef]

Disclaimer/Publisher's Note: The statements, opinions and data contained in all publications are solely those of the individual author(s) and contributor(s) and not of MDPI and/or the editor(s). MDPI and/or the editor(s) disclaim responsibility for any injury to people or property resulting from any ideas, methods, instructions or products referred to in the content.